Entrainment and suspension of sand and gravel

Jan de Leeuw[1], Michael P. Lamb[1*], Gary Parker[2,3], Andrew J. Moodie[4], Dan Haught[5], Jeremy G. Venditti[5,6], Jeffrey A. Nittrouer[4]

[1] Division of Geological and Planetary Sciences, California Institute of Technology, Pasadena, CA 91125, USA
[2] Ven Te Chow Hydrosystems Laboratory, Department of Civil and Environmental Engineering, University of Illinois at Urbana-Champaign, Champaign, IL 61801, USA
[3] Department of Geology, University of Illinois at Urbana-Champaign, Champaign, IL 61801, USA
[4] Department of Earth, Environmental and Planetary Sciences, Rice University, Houston, TX 77005
[5] Department of Geography, Simon Fraser University, Burnaby, British Columbia, Canada
[6] School of Environmental Science, Simon Fraser University, Burnaby, British Columbia, Canada

*Correspondence to: Michael P. Lamb (mpl@gps.caltech.edu)

Abstract. Entrainment and suspension of sand and gravel is important for the evolution of rivers, deltas, coastal areas and submarine fans. The prediction of a vertical profile of suspended sediment concentration typically consists of assessing 1) the concentration near the bed using an entrainment relation and 2) the upward vertical distribution of sediment in the water column. Considerable uncertainty exists in regard to both of these steps, and especially the near-bed concentration. Most entrainment relations have been tested against limited grain-size specific data, and no relations have been evaluated for gravel suspension, which can be important in bedrock and mountain rivers. To address these issues, we compiled a database with suspended sediment data from natural rivers and flume experiments, taking advantage of the increasing availability of high-resolution grain-size measurements. We evaluated 12 dimensionless parameters that may determine entrainment and suspension relations, and applied multivariate regression analysis. A best-fit two-parameter equation ($r^2 = 0.79$) shows that near-bed entrainment, evaluated at 10% of the flow depth, decreases with the ratio of settling velocity to skin-friction shear velocity to (w_{si}/u_{*skin}), as in previous relations, and increases with Froude number (Fr), possibly due to its role in determining bedload-layer concentrations. We used the Rouse equation to predict concentration upward from the reference level, and evaluated the coefficient β_i, which accounts for differences in the turbulent diffusivity of sediment from the parabolic eddy viscosity model used in the Rouse derivation. The best-

fit relation for β_i ($r^2 = 0.40$) indicates greater relative sediment diffusivities for rivers with greater flow resistance, possibly due to bed-form induced turbulence, and larger w_{si}/u_{*skin}; the latter dependence is nonlinear, and therefore different from standard Rousean theory. In addition, we used empirical relations for gravel saltation to show that our relation for near-bed concentration also provides good predictions for coarse-grained sediment. The new relations extend the calibrated parameter space over a wider range in sediment sizes and flow conditions as compared to previous work, and result in 95% of concentration data throughout the water column predicted within a factor of nine.

1 Introduction

Suspension of sediment by water plays a critical role in the dynamics of rivers, river deltas, shallow marine environments, and submarine canyons and fans. For example, suspended sediment dominates the load of lowland rivers and builds land in subsiding river deltas and coastal landscapes (Ma et al., 2017; Syvitski et al., 2005). Transport of sediment on the continental shelf is dominated by suspension of mud and sand due to wave and current bottom traction (Cacchione et al., 1999; Nittrouer et al., 1986). Suspended sediment provides the negative buoyancy of turbidity currents that move sand and gravel to the deep sea. Suspension of gravel is important in large floods, such as outburst floods (Burr et al., 2009; Larsen and Lamb, 2016), and in steep mountain canyons (Hartshorn et al., 2002), where it can contribute to bedrock erosion (Lamb et al., 2008a). Suspended sediment transport also is important in landscape engineering, such as river restoration (Allison and Meselhe, 2010), fish habitat (Mutsert et al., 2017), and the capacity of dams and reservoirs (Walling, 2006). The balance between entrainment and deposition from suspension determines patterns of deposition and erosion in these environments and therefore controls landform morphology and stratigraphic evolution (Garcia and Parker, 1991; Paola and Voller, 2005). To predict suspended sediment flux across these environments, we need robust theory for the entrainment of sediment from the bed and the vertical distribution of suspended sediment in the water column.

We focus here on understanding the suspended sediment load of cohesionless grains that are entrained from the bed (i.e., suspended bed material), rather than wash load. Most models for sediment suspension are based on application of Rouse theory (Rouse, 1937; Vanoni, 1946),

$$\frac{C}{C_a} = \left[\frac{\frac{H-z}{z}}{\frac{H-a}{a}} \right]^P, \tag{1}$$

where C [L^3/L^3] is the volumetric sediment concentration at elevation (z [L]) above the bed, C_a [dimensionless] is the reference near-bed concentration at $z = a$ [unit: L] and, H [L] is the flow depth. P denotes the dimensionless Rouse number,

$$P = \frac{w_s}{\beta \kappa u_*}, \tag{2}$$

in which w_s [L/T] is the particle settling velocity, κ is the dimensionless von Karman constant of 0.41, u_* [L/T] is the bed shear velocity and β is a dimensionless factor that accounts for differences between turbulent diffusivity of sediment and the parabolic eddy viscosity model used to derive the Rouse equation (e.g. Graf and Cellino, 2002). Although more sophisticated models exist, some of which abandon the Rouse theory entirely in favor of a more rigorous turbulence model (Mellor and Yamada, 1982), the Rouse equation remains a useful and tractable approach for modeling and field application (Graf and Cellino, 2002; van Rijn, 1984; Wright and Parker, 2004b). The Rouse equation was derived assuming an equilibrium suspension where the upwards volumetric flux of sediment per unit area due to turbulence (F_z [L/T]) is balanced by a downwards gravitational settling flux ($C w_s$) (Fig. 1) (Rouse, 1937). It predicts the shape of the concentration-depth profile, with a greater gradient in concentration for larger P (Fig. 1). By mass balance, the difference between entrainment, F_{za}, and settling, $C_a w_s$, fluxes per unit area near the bed (at $z = a$) controls the bed deposition rate, dz_b/dt [L/T] (Parker, 1978), i.e.,

$$(1 - \lambda) \frac{dz_b}{dt} = F_{za} - C_a w_s = w_s (E_s - C_a), \tag{3}$$

where λ [dimensionless] is the bed porosity, and $E_s \equiv F_{za}/w_s$ is a dimensionless sediment entrainment rate or entrainment parameter (Garcia and Parker, 1991). At steady state, Equation (3) reduces to $C_a = E_s$; thus, the near-bed entrainment rate, E_s, is necessary both to predict the vertical distribution of suspended sediment at steady state (i.e., C_a in Eq. (1)), and the rate of erosion and deposition for disequilibrium suspensions (Eq. (3)).

Application of Eqs. (1) – (3) requires specification of β, E_s and a, and the approach in previous work has been to identify important dimensionless variables and fit data from flume experiments and natural rivers to these variables (e.g., Smith and McLean, 1977; van Rijn, 1984; Garcia and Parker, 1991). Owing to differences in datasets analyzed and the dimensionless variables explored, there is considerable deviation in the form of previous models and their predictions (Figs. 2 & 3, Table 1 & 2). For example, Einstein (1950), Engelund and Fredsøe (1976), van Rijn (1984) and Smith and McLean (1977) used a relation for a that depends primarily on grain diameter (D [L]), and secondarily on u_*/w_s or Shields number, $\tau_* = \tau_b/(\rho_s - \rho_w)gD$ (where τ_b [ML^{-1}T^{-2}] is bed stress, ρ_s [M/L^3] is sediment density and ρ_w [M/L^3] is fluid density). Their rationale was based on the idea that there is a well-mixed near-bed zone of bedload transport, and that suspended sediment is entrained from this zone (Fig. 1B). Thus, they developed relations for a that scale with the height of bedload saltation. In contrast, Garcia and Parker (1991) and Wright and Parker (2004b) argued for a simpler approach and used a reference height that is a small fraction of the flow depth, and they proposed $a = 0.05H$ as a useful reference height, with no dependence on D.

In practice the factor β is often neglected (i.e., $\beta = 1$) under the assumption that the parabolic eddy viscosity assumption used to derive Eq. (1) represents well the turbulent transport of fine suspended sediment. $\beta < 1$ in Eq. (2) has been attributed to damping of turbulence due to sediment-induced stratification, which alters the eddy viscosity (Einstein, 1955; Graf and Cellino, 2002; Wright and Parker, 2004a), and to flocculation, which increases the settling velocity of fine-grained sediment (e.g. Bouchez et al., 2011; Droppo and Ongley, 1994). Some formulas (van Rijn, 1984; Santini et al., 2019) and datasets (Graf and Cellino, 2002; Lupker et al., 2011) indicate $\beta > 1$, which implies enhanced mixing of sediment relative to momentum (Table 1; Fig. 2). Graf and Cellino (2002) showed that turbulence generated by bedform roughness results in better sediment mixing and thus in a higher β. Field and flume data (Chien, 1954; Coleman, 1970; van Rijn, 1984) indicate that β is greater than unity for the coarse grain-size fraction of the suspended material (Greimann and Holly Jr, 2001). Nielsen and Teakle (2004) argued that the Fickian diffusion model in the derivation of the Rouse equation is not valid for steep concentration

gradients, resulting in $\beta > 1$. Most previous relations show a trend of decreasing β with increasing u_*/w_s (van Rijn, 1984; Graf and Cellino, 2002; Wright and Parker, 2004b) (Fig. 2a), which could be due to turbulence damping associated with high concentration suspensions. Wright and Parker (2004b) showed that β is also a function of reference concentration divided by slope (C_a/S) (Fig. 2b), which they attributed to sediment stratification. Santini et al. (2019) found that β is a function of u_*/w_s and the ratio between flow depth and bed grain size (H/D) (Fig. 2c).

Compared to β, even larger uncertainty exists the dimensionless entrainment rate, E_s. In previous work E_s was assessed by measuring the near-bed concentration for equilibrium suspensions, since $E_s = C_a$ under those conditions (i.e., $\frac{dz_b}{dt} = 0$ in Eq. 3). Previous work found that C_a was a function of bed stress and grain size (Fig. 3; Table 2) (Einstein, 1950; Engelund and Fredsoe, 1976; Smith and McLean, 1977; van Rijn, 1984; Cedik and Rodi, 1984; Akiyama and Figushima, 1986, Garcia and Parker, 1991; Wright and Parker, 2004b). While holding bed stress constant, most relations predict smaller C_a with increasing grain size across the sand regime, as expected, but some surprisingly show increasing C_a for coarse sands and gravel (Akiyama and Figushima, 1986, Garcia and Parker, 1991; Wright and Parker, 2004b) (Fig. 3a, 3c). Due to the greater weight and settling velocity of larger particles, this behavior is unrealistic and likely occurs because these coarse particles are outside of the data range used to fit the relations. Despite the importance of gravel suspension in steep mountain rivers and megafloods, data do not exists to evaluate the models in the gravel regime. All relations show increasing C_a with bed stress, as expected, but there are orders of magnitude differences in the predictions for C_a (Fig. 3b). Part of this deviation is due to differences in the reference level ($z = a$) (Fig. 3b); but even when using a common reference level ($a = 0.05H$; Fig. 3d), significant variability still exists. Some of the variance is also due to extrapolating the models beyond the range in which they were calibrated; for example, van Rijn (1984) predicts concentrations greater than 100% at high shear stresses.

We revisited the problem of sediment entrainment and suspension of cohesionless bed sediment by compiling a large database of sediment-size specific data for bed-sediment mixtures, testing existing

relations against the database, and proposing improved relations for E_s and P. Several existing formulas for E_s are applicable only to uniform sized bed sediment (Akiyama, 1986; Celik and Rodi, 1984; Einstein, 1950; Engelund and Fredsøe, 1976; van Rijn, 1984; Smith and Mclean, 1977) (Table 2). However, given the strong control of grain size on near-bed concentrations, accurate formulas likely need to make grain-size specific predictions for sediment mixtures (Garcia and Parker, 1991; McLean, 1992; Wright and Parker, 2004b). Our database takes advantage of high resolution grain-size measurements using laser diffraction (Lupker et al., 2011; Gitto et al., 2017; Haught et al., 2017; Santini et al., 2019), which allow a single concentration profile to be separated into many grain-size specific concentration profiles. Our dataset also contains a wide range grain sizes, extending into the silt regime (median bed sizes range from 44 μm to 517 μm), and expands on the number of field measurements compared to previous efforts. We are unaware of studies on C_a for gravel, but data does exist for saltation heights, velocities and bedload fluxes for gravel, and calibrated relations for these variables also exist (Chatanantavet et al., 2013; Sklar and Dietrich, 2004). To attempt to better constrain suspension of very coarse sand and gravel, we used existing semi-empirical saltation theory for gravel to check for consistency between sand suspension data and what might be expected for near-bed gravel concentrations.

2 Methods

2.1 Suspended sediment profiles

Based on previous theory, we searched for available datasets from rivers and flume experiments that had suspended sediment profiles ($C(z)$), depth-averaged flow velocity (U), flow depth (H), channel bed slope (S) bed material grain-size (D), and the grain-size distribution of the bed material and suspended sediment samples (Table 3; Table S1). Some of the experimental studies used a narrow grain-size distribution, and, like previous work, we assumed that the sediment distribution from these studies was uniform. Many of the older datasets were used in empirical regressions from previous relations (e.g. Garcia and Parker, 1991; van Rijn, 1984; Wright and Parker, 2004b). In addition, we used a river dataset from the Yellow River (Moodie, 2019), which provides a fine-grained end member. In total, our database contains 180 concentration profiles from 8 rivers and 62 profiles from 6 different experimental studies. We analyzed

only the grain fractions coarser than 62.5 μm (i.e., sand). The mud fraction was present on the bed only in small amounts, and following previous work, mud was assumed to require a different approach, potentially due to supply limitation (Garcia, 2008), cohesion or flocculation. Grain-size distributions in older studies were determined from sieve analysis of bed material and suspended sediment samples. The more recent studies used laser diffraction techniques, which have the advantage that a larger number of grain-size classes can be distinguished. We calculated the grain-size specific suspended sediment concentration (C_i) using

$$C_i = f_i C_{tot}, \tag{4}$$

where f_i [dimensionless] is the mass fraction of grains of the i-th size and C_{tot} is the total suspended sediment concentration for all sizes. In addition, we computed the D_{50} (median grain size) and D_{84} of the bed material using linear interpolation between the logarithm of D and the cumulative size distribution.

Concentration profiles in the database typically contain 3 to 8 measurements in the vertical dimension. The Rouse profile was fitted to the profile data for each grain-size class in log-transformed space using linear least squares to find P_i (Fig. 4a). Confidence bounds (68%; 1 σ) for the fitted coefficients were obtained using the inverse R factor from QR decomposition of the Jacobian. Data were excluded from further steps in the analysis if the ratio between the upper and lower bound of the confidence interval was greater than 10 or smaller than 0.01, as these data do not follow a Rouse relation for unknown reasons (e.g., measurement error), and would appear as sparse outliers. Of the data analyzed, 201 points (15%) were excluded based on these criteria. Some studies (Bennett et al., 1998; Muste et al., 2005) have shown that P (or β) can vary over the flow depth, but this effect cannot be incorporated into our approach; instead we found one value of P_i that best fit the concentration profile for each grain size class.

We used the Rouse equation (Eq. 1) for each grain-size class to extrapolate or interpolate the concentration to a reference level at 10% of the flow depth, i.e., we set $a = 0.1H$ and $C_{ai} = C_i(z = a)$. Extrapolation to very near the bed can be difficult due to large concentration gradients and poorly constrained near-bed processes such as interactions with bedforms. However, a reference level that is too far away from the bed may poorly capture the exchange of sediment with the bed. Previous researchers used reference levels

that were either at some fraction of the flow depth (Akiyama, 1986; Celik and Rodi, 1984; Garcia and Parker, 1991; Wright and Parker, 2004b) or that were related to the bed roughness height (Einstein, 1950; Engelund and Fredsøe, 1976; Garcia and Parker, 1991; Smith and Mclean, 1977) (Table 2). We explored the collapse of the entrainment data for both types of reference levels. For each reference level, we fit our preferred and best-fitting two-parameter entrainment relation (as described in the Results) to the data with u_{*skin}/w_{si} as its first parameter and Froude number as the second parameter. We found that a reference level at a fraction of the flow depth gave a better collapse of the entrainment data than a reference level related to the saltation layer height. Furthermore, we also tested different flow-depth fractions and found that the fit improved, in a least-squared sense, as the reference level moved to a larger fraction of the flow depth (Fig. 4B). However, there is little change in r^2 once the reference level is higher than ~10% of the flow depth. Therefore, we used a reference level at 10% of the flow depth for all results shown below.

For sediment mixtures, the grain-size specific near-bed concentration is partially controlled by the fraction of each grain-size class in the surface bed material. To account for this effect, Garcia and Parker (1991) introduced an entrainment rate (E_{si}) for each grain-size class that is linearly weighted by the fraction of that material in the bed:

$$E_{si} = \frac{C_{ai}}{F_{bi}},$$ (5)

where C_{ai} is the near-bed concentration of that grain-size class and F_{bi} is the mass fraction of bed material that falls in that grain-size class. For uniform sediment, the entrainment rate (E_{si}) is equivalent to the near-bed concentration (C_{ai}).

2.2 Independent parameters and profile fitting

Here we review the independent parameters that we evaluated for dependencies with dimensionless entrainment rate, E_{si}, and for β_i in the Rouse number. The primary group of parameters describes the ratio between bed stress and grain size or grain settling velocity. These parameters include the ratio between shear velocity and settling velocity (u_*/w_s), where we evaluated the total shear velocity as,

$$u_* = \sqrt{\tau_b/\rho_w} = \sqrt{gHS},$$ (6)

assuming steady, uniform unidirectional flow. Others have proposed that entrainment depends on the skin-friction portion of the total shear stress, u_{*skin}, rather that the total shear stress. To estimate u_{*skin}, we used the Manning-Strickler relation,

$$\frac{U}{u_{*skin}} = 8.1 \left(\frac{H_{sk}}{k_s}\right)^{1/6},$$ (7)

where $k_s = 3\ D_{84}$ is the grain roughness on the bed, H_{sk} is the depth due to skin friction and $u_{*skin} = \sqrt{gH_{sk}S}$ (e.g., Wright and Parker, 2004b). To calculate the particle settling velocity, we followed Ferguson and Church (2004) for each grain-size class,

$$w_{si} = \frac{RgD_i^2}{C_1v + (0.75C_2RgD_i^3)^{0.5}},$$ (8)

in which $R = (\rho_s - \rho_w)/\rho_w$ is the submerged specific density of sediment, v is the kinematic viscosity of the fluid, $C_1 = 18$ and $C_2 = 1$ are constants set for natural sediment, D_i is the grain diameter within the size class of interest. Another parameter that relates to the ratio between bed stress and gravity acting on the grains is the Shields number,

$$\tau_* = \frac{\tau_b}{(\rho_s - \rho)gD_i},$$ (9)

and we again assumed steady, uniform flow to find $\tau_b = \rho gHS$. Similar to the shear velocity, it is also possible to calculate a Shields number for the skin-friction component of the total shear stress,

$$\tau_{*skin} = \frac{\tau_{skin}}{(\rho_s - \rho)gD_i},$$ (10)

where $\tau_{skin} = \rho u_{*skin}^2$ by definition. Shields numbers can be rewritten in terms of u_*/w_{si} through use of a particle drag coefficient,

$$C_d = \frac{RgD_i}{w_{si}^2},$$ (11)

which we also evaluated (i.e., $\tau_* = \frac{\tau_b}{(\rho_s - \rho)gD_i} = \left(\frac{u_*}{w_{si}}\right)^2 \frac{1}{C_d}$).

The next group of parameters describes dimensionless particle sizes, including the particle Reynolds number,

$$R_p = \frac{u_*D_i}{v}.$$ (12)

Likewise, this parameter can also be calculated with the skin-friction component of the shear velocity,

$$R_{p,skin} = \frac{u_{*skin}D_i}{\nu}. \tag{13}$$

A particle Reynold number can be defined without shear velocity as,

245

$$Re_p = \frac{\sqrt{RgD_i}D_i}{\nu}. \tag{14}$$

For sediment mixtures, the relative particle size might play a role due to hiding and exposure effects (Garcia and Parker, 1991; Wright and Parker, 2004b); this effect can be captured with $\frac{D_i}{D_{50}}$. Sediment-induced density stratification can decrease entrainment by damping near-bed turbulence, and this effect is thought to be most important in deep, low gradient rivers (Wright and Parker, 2004b). Wright and

250 Parker (2004b) proposed that the ratio of near-bed concentration to bed slope is a good predictor for stratification, $\frac{C_a}{S}$, where they used C_a at 5% of the flow depth. Large, low gradient rivers also have small Froude numbers and low bed slopes, so we evaluated Froude number and slope as additional parameters. Froude number was calculated as:

$$Fr = \frac{U}{\sqrt{gH}}. \tag{15}$$

255 The entrainment rate could also be affected by turbulence or changes to the boundary layer from bed roughness or bedforms, which tend to correlate with a flow resistance friction coefficient (e.g., Engelund and Hansen, 1967),

$$C_f = \frac{u_*^2}{U^2}. \tag{16}$$

260 We also evaluated H/D_{50} as a proxy for flow resistance due to grain roughness.

In order to find relations that explain the variation in our best fit E_{si} and P_i values from the vertical concentration profiles, we regressed the E_{si} and P_i values against the 12 variables described above (Eq. 6 – 16). In some applications, like reconstructing flow conditions from sedimentary strata, it is useful to

265 have an entrainment relation that depends on u_{*skin}, while for forward modeling a relation based on u_* is preferred. The two shear velocities are highly correlated; therefore, we explored two versions of the fit relations using either u_* or u_{*skin}, but not both at the same time. Because the Rouse parameter, P_i, by

definition depends inversely on u_*/w_{si} (or u_{*skin}/w_{si}) (Eq. 2), we found the best fit relations for P_i rather than β_i to avoid spurious correlation. We then solved for the equivalent relation for β_i using the

270 definition of P_i (Eq. 2). We started the analysis by testing all models with one explanatory variable and ranked the models according to the coefficient of determination from linear least squares regression (r^2) evaluated in log-log space. Next, a second parameter was used in addition to first best-fitting parameter and the resulting two-parameter models were ranked according to r^2. The procedure was repeated with additional parameters until the increase in r^2 was smaller than 0.04. For the fitting of multi-parameter

275 models, we varied the exponents on each parameter in the model simultaneously to find the combination of exponents that yielded the best fit. This approach gave a higher r^2 compared to the stepwise approach used in previous work (e.g., Garcia and Parker, 1991) of first fitting the dominant variable and then fitting the secondary variables to the residuals. In addition, we tested fitting with the York method (Table S2), which gives less weight to data with large errors (York, 1968), but found only minor differences and so

280 all results presented use the simpler linear least-squares method. All parameters were used to evaluate relations for E_{si} and β_i, except for D_i/D_{50} , which we used for only E_{si} since it is relevant for particle-particle interactions at the bed surface. In the results we report two versions of the best fitting one, two and three parameter models: one version that is based on the total bed shear stress and one version that is based on the skin-friction component of the bed shear stress. Model fits using all possible combinations

285 of the input parameters are given in Table S2.

2.3 Comparison to theory for gravel

Although gravel suspension is important in bedrock and steep mountain rivers, and during megafloods, we are not aware of datasets of near-bed concentration in the gravel range. Following previous work (McLean, 1992; Lamb et al., 2008a), our approach was to derive the near-bed concentration in the bedload

290 layer, and then use Rouse theory to predict that concentration at $0.1H$ to compare with the sand dataset (e.g., Fig. 1B).The near-bed volumetric concentration within the bedload layer can be calculated by continuity as

$$C_b = \frac{q_b}{(H_b U_b)}, \tag{17}$$

where q_b [L²/T] is the volumetric bedload flux per unit width, H_b [L] is the bedload layer thickness and U_b [L/T] is the bedload velocity. Most relations for bedload flux take the form

$$\frac{q_b}{\sqrt{(RgD^3)}} = a(\tau_* - \tau_{*c})^b, \qquad (18)$$

where a and b are empirical constants, which we set to $a = 5.7$ and $b = 1.5$ (Fernandez Luque and van Beek, 1976), and τ_{*c} is the critical Shields number at initial motion, which we set to Lamb et al. (2008b)

$$\tau_{*c} = 0.15S^{0.25}. \qquad (19)$$

The bedload layer height and velocity were determined from Chatanantavet et al. (2013). They compiled a large dataset of gravel saltation observations and found a good fit with the following relations:

$$\frac{U_b}{U} = 0.6 \qquad , \qquad (20)$$

$$\frac{H_b}{H} = 0.6\left(Fr\left(\frac{D_i}{H}\right)^2\right)^{0.3}. \qquad (21)$$

Equations (17) – (21) were combined with a flow resistance relation (Eq. 7, assuming no form drag) and $C_d = 0.7$ for gravel (Lamb et al., 2017) to calculate C_b in the bedload layer using a numerical iterative scheme. Manipulating the equations revealed that C_b is a function of only τ_* and Fr. To calculate C_a for gravel, we extrapolated the concentration profile (Fig. 1b) from the top of the saltation layer to $0.1H$ using the Rouse equation (Eq. 1). To obtain the Rouse number, we used our best-fit one-parameter model that uses total shear velocity (u_*) (see Table 4). We then used a wide range of input parameters ($0.1 < Fr < 1$ and $1 < \tau_* < 1000$) relevant to suspension of gravel in mountain rivers and large floods to predict a range of expected values of C_a for gravel. Although Eqs. (20) and (21) have not been tested for high Shields numbers in the suspension regime, they have reasonable limiting values ($U_b = 0.6U$, $H_b = H$) and provide a starting place to compare sand entrainment and gravel saltation theories.

3 Results

3.1 Rouse number, P_i

Equation (1) was fit to the concentration profile data where P_i was treated as a fitting parameter. Then P_i was regressed against the hypothesized controlling variables (Eqs. 11-16). Figure 5 and Table 4 show the results for P_i including our best fitting one-, two- and three-parameter models. The variable with the most

explanatory power is u_*/w_{si} ($P_i = (u_*/w_{si})^{-0.45}$; $r^2 = 0.33$). The best-fit two-parameter model that
includes C_f is better than the predictions of the one-parameter model ($r^2 = 0.40$). Going from a two-parameter model to a three-parameter model brings a smaller improvement ($r^2 = 0.43$). Therefore, we recommend the two-parameter model for combined accuracy and simplicity:

$$P_i = 0.145 \left(\frac{u_{*skin}}{w_{si}}\right)^{-0.46} C_f^{-0.3},$$ (22)

although there are a number of models using different variables that yield similar r^2 values (Table S2),
and some combinations might be preferred over others depending on the application. Eq. (22) indicates
that sediment is better mixed in the water column with larger u_{*skin}/w_{si} and with larger bed roughness
coefficient, C_f. Equation (22) performs well compared to previous relations, as is shown by a boxplot of
measured-to-predicted ratios (Fig. 6). For the best-fit two-parameter model, the measured-to-predicted
ratio falls between 0.74 and 1.29 for 50% of the data. Using a Rouse number with a constant $\beta = 0.94$
also provides a reasonably good fit and an improvement over several more involved relations (Fig. 6).

Equation (22) can be rewritten for β_i using Eq. (2), and by assuming that u_* in Eq. (2) is actually u_{*skin},
as

$$\beta_i = 17.24 \left(\frac{u_{*skin}}{w_{si}}\right)^{-0.54} C_f^{0.3},$$ (23)

Because some of the dimensional quantities appear in multiple dimensional variables, and because the
dimensional variables are not necessarily independent from each other, we tested for spurious correlations
by rearranging the two-parameter relation for β_i to isolate the dimensional dependencies on grain size
and skin-friction shear velocity (Fig. 7). The data and our model show a decrease in suspended sediment
mixing in the water column with larger grain sizes, as expected (Fig 7a). Previous relations show the same
trend, but the relations of van Rijn (1994) and Graf and Cellino (2002) have stronger dependencies in the
sand regime. Suspended sediments are better mixed with increasing skin-friction shear velocity (Fig. 7b).
The data suggest that P_i varies proportionally to $u_*^{-0.4}$ whereas standard Rouse theory (Eq. 2) indicates
that P_i is proportional to u_*^{-1}.

3.2 Dimensionless entrainment rate, E_{si}

Results for the best fit dimensionless entrainment rate is shown in Figure 8 and Table 5, and all possible variable combinations are given in Table S1. The following one-parameter relation gives the best fit with the data for E_{si} ($r^2 = 0.61$) (Fig. 8a):

$$E_{si} = 4.23 \times 10^{-5} \left(\frac{u_{*skin}}{w_{si}} \right)^{1.94}. \tag{24}$$

Froude number was the most significant second parameter:

$$E_{si} = 4.74 \times 10^{-4} \left(\frac{u_{*skin}}{w_{si}} \right)^{1.77} Fr^{1.18}, \tag{25}$$

which has a significantly better fit ($r^2 = 0.79$) than the best fitting one-parameter relation (Fig. 8b). Addition of a third variable to the model gives little further improvement of the fit (Fig. 8c; $r^2 = 0.80$), and many of the variables used as a third parameter give a similar level of improvement (Table S1). Using Eq. (25), 80% of the entrainment data is predicted within a factor of 3 (Fig. 8b; Fig. 9). Along with our proposed new relation (Eq. 25), we also compared the dataset against the previous relations (Fig. 9). The boxplots in Figure 9 highlights that some relations systematically under predict (Wright and Parker, 2004b) or over predict entrainment rate (Garcia and Parker, 1991). In addition, previous relations have a larger spread in measured-to-predicted ratios than Eq. (25). To check for spurious correlation in the dimensionless variables, we rearranged our two-parameter entrainment relation (Eq. 25) to isolate the dependencies of entrainment rate on grain size (Fig. 10a) and skin-friction shear velocity (Fig. 10b). Our relation indicates that entrainment depends on grain size to the -3.1 power in the sand range, whereas previous relations suggest a much weaker dependence. Compared to previous work, our relation also suggests a relatively weak dependence on skin-friction shear velocity ($E_{si} \propto u_{*skin}^{1.77}$).

Similar to Garcia and Parker (1991) and Wright and Parker (2004b), we modified equation (25) such that the predicted entrainment rate is limited at 0.3, as total suspended sediment concentrations greater than 30% by volume are not physically reasonable for dilute, turbulent flows. In addition, a threshold (0.015), best fit by eye, was added to the entrainment relation because the concentration data fall below the trend of the regression relation at the lower flow strengths (Fig. 8b), suggesting a threshold of significant sediment entrainment at the reference level. The resulting equation has the following form (Fig. 8b):

$$E_{si} = \frac{4.74 \times 10^{-4} \left(\left(\frac{u^*_{skin}}{w_s} \right)^{1.5} Fr - 0.015 \right)^{1.18}}{1 + 3 \left(4.74 \times 10^{-4} \left(\left(\frac{u^*_{skin}}{w_s} \right)^{1.5} Fr - 0.015 \right)^{1.18} \right)}.$$
(26a)

The equivalent formula for the best-fit two parameter model without a form drag correction (Table 5) is

$$E_{si} = \frac{7.04 \times 10^{-4} \left(\left(\frac{u^*}{w_s} \right)^{0.945} Fr - 0.05 \right)^{1.81}}{1 + 3 \left(7.04 \times 10^{-4} \left(\left(\frac{u^*}{w_s} \right)^{0.945} Fr - 0.05 \right)^{1.81} \right)}$$
(26b)

3.3 Predicting sediment concentration

375   In Sections 3.1 and 3.2 we found the best-fit models for the dimensionless entrainment rate (E_{si}) and Rouse number (P_i). However, ultimately, we want to predict sediment concentration throughout the water column, and the best-fit models for (E_{si}) and (P_i) do not necessarily combine to yield the best-fit model for sediment concentration owing to non-linearity in E_{si}, P_i and the Rouse equation (Eq. 1). Here we used different combinations of our preferred one-, two- and three-parameter models for entrainment (E_{si}) and

380   Rouse number (P_i) to predict the grain-size specific concentrations at each data point in the water column for all our entries in the database, and assessed model performance (Table 6). The concentration predictions improve as more parameters are added to the entrainment model, whereas a Rouse model with more than one parameter makes the predictions worse (Table 6). Our preferred model for concentration throughout the water depth uses the two-parameter model to predict the entrainment rate ($E_{si} = 4.74 \times$

385   $10^{-4} \left(\frac{u_{*skin}}{w_{si}} \right)^{1.77} Fr^{1.18}$) and the one-parameter model for the Rouse number ($P_i = (u_*/w_{si})^{-0.45}$) (Fig 11). Such a model gives significantly better predictions than the most basic formulation that uses one-parameter models for entrainment and Rouse number (r^2 of 0.87 versus 0.65; Table 6). The goodness of fit also is fairly constant over the height of the flow; the upper 1/3 of the flow has a slightly lower r^2 (0.80) than the predictions from the lowest 1/3 of the flow ($r^2 = 0.89$) (Fig. 11). Ninety five percent of the data

390   are predicted within a factor of 9.

3.4 Extension to gravel

The suspended sediment data that we used to calibrate the entrainment relation covers material in the sand range. To evaluate how our entrainment relation performs for coarser suspended sediment, we used the empirical saltation equations for gravel to infer bedload-layer concentrations, C_b, and interpolated these to the reference level ($0.1H$) to infer C_a for gravel (Section 2.3). Importantly, the gravel concentrations at the reference height can be predicted from the saltation model (Section 2.3) using only the independent parameters of Fr and τ_*, similar to our best fitting two-parameter entrainment model. To compare to gravel, we assumed a uniform sediment size and used the version of our best-fit two parameter model that does not include a form-drag correction (Eq. 26b). This was done because the gravel saltation studies typically were performed over a planar bed, whereas form drag likely played a significant role in the sand data sets owing to dunes. The marked parameter space on Figure 12 shows the expected range of C_b and C_a for a wide range of model input parameters for gravel: $0.1 < Fr < 1$ and $1 < \tau_* < 1000$. Predicted concentrations in the gravel bedload layer are up to several orders of magnitude higher than the predictions from our entrainment relation at 10% of the flow depth (Fig. 12). However, due to the rapid decrease of sediment concentration away from the bed predicted by the Rouse profile, the concentration inferred at $0.1H$ for gravel overlaps with the empirical relation for sand, implying that Eq. (26b) might also be a good predictor of gravel entrainment.

4 Discussion

4.1 Physical rationale for model dependencies

The explanatory variables in the models for P_i and β_i are u_{*skin}/w_{si} and C_f. The dependency on these parameters could reflect processes that result in the turbulent diffusivity for suspended sediment being different from the parabolic relation used in the derivation of the Rouse profile (e.g., Bennett et al., 1998). Compared to standard Rouse theory, in which the Rouse parameter is inversely dependent on u_{*skin}/w_{si} (or u_*/w_{si}), our results indicate a significant non-linearity. Our one-parameter model indicates that concentration profiles are better mixed than standard theory for small u_*/w_{si} and are more stratified for larger u_*/w_{si}, with a transition point at about $u_*/w_{si} = 7$, corresponding to $\beta_i = 1$. Sediment-induced

stratification is often cited (Winterwerp, 2006; Wright and Parker, 2004b, 2004a) as a factor that decreases mixing of sediment (i.e. $\beta < 1$). This effect is particularly important when absolute concentration is high, and may help explain why our best-fit model is more stratified (i.e. $\beta < 1$) than standard Rousean theory

420   for large u_*/w_{si}. An alternative hypothesis by Nielsen and Teakle (2004) is that for steep concentration gradients, the size of the turbulent eddies is large relative to the mean height of sediment in the flow. Under these circumstances, large eddies might more effectively mix sediment that is concentrated close to the bed. This process may explain the better mixed concentration profiles we observed (i.e., $\beta_i > 1$), as compared to standard theory, at small u_*/w_{si} when near-bed concentration gradients are large.

425

Our relation implies that β_i correlates positively with the flow friction coefficient C_f. This dependency could be from bedforms; bedforms increase C_f due to form drag (Engelund and Hansen, 1967), and they may also increase the vertical mixing of sediment by deflecting transport paths up the stoss side of dunes and mixing suspended sediment in the turbulent wake in the lee of dunes. Similarly, Santini et al. (2019)

430   found that β correlated positively with H/D (Fig. 2c), which is another measure for bed roughness in flows without bedforms. In agreement, Graf and Cellino (2002) reviewed a number of experimental studies and found that $\beta < 1$ for experiments without bedforms and $\beta > 1$ for experiments with bedforms. Flow resistance (C_f) also can be smaller in flows with sediment-induced stratification, which correlates with smaller β_i (e.g., Wright and Parker, 2004a).

435

Our new empirical relation for sediment entrainment suggests that only u_{*skin}/w_{si} (or u_*/w_{si}) and Fr are needed to predict entrainment rate, similar to the forward model we developed for the suspension of gravel (Section 2.3). The ratio u_{*skin}/w_{si} describes the fluid forces relative to gravitational settling; similar parameters have appeared in all previous relations that we reviewed (Table 2). The reason for the

440   increase in entrainment with Froude number is less clear. A small Froude number implies a deep and low-gradient flow, and Froude numbers are typically smaller in natural rivers compared to flume experiments. Wright and Parker (2004b) introduced an entrainment relation with a bed slope dependency and argued that entrainment in large low sloping rivers is reduced due to stratification effects. Sediment-induced stratification causing damping of turbulence might be the cause of the Fr dependency in our relation.

445 Regardless, we found a better fit with the data using Fr than using $\frac{C_a}{S}$ or S (Table S2), the parameters suggested by Wright and Parker (2004b). Froude number also might influence the size and shape of bedforms (Vanoni, 1974), which can affect boundary layer dynamics and near-bed turbulence, and surface waves. The Froude number is the ratio between inertial to gravitational forces, or more formally the ratio of a unidirectional flow velocity to the celerity of a shallow water wave (i.e., $Fr = U / \sqrt{gH}$). However,

450 we do not think these are the reasons why the dependence of E_{si} on Fr emerges in our analysis; rather, our forward model (Section 2.3) suggests that it emerges as a controlling parameter because of the role of U and H in determining bedload layer concentrations, which is discussed in more detail in Section 4.3.

Many of the dimensionless parameters we evaluated correlate with each other in rivers. While u_{*skin}/w_{si}

455 or u_*/w_{si} were consistently the dominant variables, several of the possible secondary variables had similar explanatory power as the ones given in our preferred models. For sediment entrainment, some of the more highly ranked variables are C_a/S and τ_{*skin} in one-parameter models and H/D_{50}, S and D_i/D_{50} in two parameter models; and for Rouse number they include $R_{p,skin}$ and τ_* for one-parameter models, and Re_p and C_a/S in two parameter models (Table S2). In addition, there is some systematic deviation between

460 datasets for different rivers (Fig. 8), and different parameters and exponents might better minimize residuals at specific locations. While our model has been fit to a large dataset, it has not been validated with independent data. More data is clearly needed on grain-size specific concentration profiles for equilibrium suspensions under a wide range of u_*/w_{si}, Fr and particle sizes, including coarse sand and gravel.

465 **4.2 Predicting sediment concentration below the reference level**

Combining the predictions for the grain-size specific reference concentration and Rouse parameter allows for calculation of the grain-size specific sediment concentration throughout the water column (Fig. 11). Our relation shows that the grain-size specific sediment concentration at any given elevation can be predicted to relatively high accuracy ($r^2 = 0.87$) using the preferred combination of a two-parameter

470 entrainment relation and the one-parameter Rouse number relation (Section 3.3). However, it is unclear

how to evaluate the sediment concentration below the reference level, which could constitute a significant portion of the sediment load. Bedload fluxes are notoriously difficult to estimate; further, it is unclear if the region below the reference level is entirely bedload, or if it is bedload and suspended load (e.g., Fig. 1b). Ashley et al. (2020) showed how bedload sediment fluxes can be estimated from discharge-averaged suspended sand concentrations, but their method does not predict the concentration profile. One approach might be to assume that sediment concentration is uniform below the reference level at $C_i = C_{ai}$, as might be the case in a well-mixed bedload layer (e.g., McLean, 1992) (Fig. 1b). However, this assumption is inconsistent with our analysis of the saltation equations, which shows that bedload layers should have greater concentrations and be less than 10% of the flow depth (Fig. 12), especially for sand in deep flows. A second approach is to use the Rouse profile to extrapolate towards the bed or towards the top of the bedload layer; however, this approach is also problematic because the Rouse profile predicts infinitely large concentrations at the bed. Some of our datasets had concentration measurements below the reference level (Fig. 13). The data are scattered, but the binned data points suggest a nearly constant concentration with elevation below the reference level. For lack of a better method, we propose to use the geometric mean of this data as $C_i = 1.66 C_{ai}$ to approximate the concentration-depth profile below the reference level (Fig. 13).

4.3 Extension to gravel and bedload-layer theory

The transport of sand and gravel are often modeled using different empirical formulas, which hinders modeling of systems of mixed gravel-sand transport (Wilcock and Crowe, 2003) and gravel-sand transitions (Paola et al., 1992; Lamb and Venditti, 2016). Gravel also can be in suspension in bedrock and steep mountain rivers, and during large floods (Hartshorn et al., 2002; Larsen and Lamb, 2016), and it would be useful to have an entrainment relation to model sediment transport and bedrock erosion in these settings (Lamb et al., 2008a; Scheingross et al., 2014). Unfortunately sand and gravel are often treated separately, which limits our ability to develop a unified sediment transport theory. Our entrainment relation for sand matches expectations from gravel saltation models (Fig. 12), suggesting that the entrainment relation may be used for sand or gravel, or mixtures of the two. However, we currently lack data of gravel suspension profiles, and developing methods to acquire such data should be the focus of

future efforts. It's also unclear how entrainment is complicated by bimodal mixtures (Wilcock and Crowe, 2003) and complex flow hydraulics in steep rivers with large roughness that can significantly affect lift forces and near-bed turbulence (Lamb et al., 2017).

The good fit between the modeled gravel concentrations and the measured sand data for near-bed sediment concentration suggests that the bedload layer equations (Section 2.3) might also be used to generate a forward model for near-bed sediment concentration that works for sand and gravel systems, similarly to previous efforts (e.g., McLean, 1992). To evaluate this possibility, we used the saltation equations (Eqs.17-21) to calculate sediment concentrations within the bedload layer for conditions corresponding to our dataset entries of sand bedded rivers. To extend equation (18) to grain-size mixtures, we let $D = D_i$ and $\tau_{*c} = \tau_{*ci}$ and used a hiding function (Parker et al., 1982) so that

$$\tau_{*ci} = \tau_{*c50} \left(\frac{D_i}{D_{50}}\right)^{-\gamma}, \tag{27}$$

where τ_{*c50} is the critical Shields number for the median sized bed sediment. Equation (27) accounts for hiding of smaller grains in between larger grains, which renders the smaller grains less mobile, and the exposure of larger grains into the flow, which renders them more mobile. For $\gamma = 1$, all grains in a bed mixture move at the same bed stress, while $\gamma = 0$, the critical stress for motion is proportional to grain weight. Gravel bedded rivers typically have $\gamma = 0.9$ (Parker, 1990). For sand, we evaluated the critical Shields number following Brownlie (1981)

$$\tau_{*c50} = 0.5\left[0.22\, Re_p^{-0.6} + 0.06 * 10^{\left(-7.7 Re_p^{-0.6}\right)}\right], \tag{28}$$

rather than Eq. (19), which is intended for gravel only. We then calculated the concentrations at 10% of the flow depth using the Rouse equation (Eq. 1) with the best-fit one-parameter model for the Rouse number. Although the saltation equations in Section 2.3 were calibrated for gravel, similar relations also have been used for sand (e.g., Lamb et al., 2008a).

Surprisingly, the near-bed sand concentration for the entries in our database (Section 2.1) are relatively accurately predicted by the bedload forward model without any parameter fitting (Fig. 14b). In fact, the predictions by the bedload-layer forward model are only slightly worse than the predictions by our

preferred two-parameter entrainment model (Fig. 14a) that was fit to the data (r^2 of 0.68 vs 0.87). Importantly, the forward model yields the same controlling parameters as the empirical model, namely Shields number, Froude number and the bed grain-size distribution. The forward model suggests that the dependence of E_{si} on u_{*skin}/w_{si} (or u_*/w_{si}) is predominantly because larger u_{*skin}/w_{si} correlates with larger τ_* and larger bedload-layer concentrations (Eq. 17 and 18), as well as more efficient mixing of the bedload-layer sediment up to the reference height (Eq. 1). Less intuitive is the dependence of E_{si} on Froude number. In the forward model, this dependence is because larger Fr, for the same τ_* correlates with larger D_i/H (which can be shown by manipulating Eq. 7). In turn, larger D_i/H with constant τ_* correlates with greater bedload fluxes ($q_b \propto D_i^{3/2}$ in Eq. 18), smaller bedload layer heights (due to smaller H in Eq. 21) and slower bedload layer velocities (due to smaller U in Eq. 20), all of which increase sediment concentration in the bedload layer (Eq. 17). Thus, the forward model indicates that the Fr-dependency on E_{si} emerges because bedload layer dynamics depend on U and H, and explanations for this dependency that rely on stratification, bedforms or surface waves are not necessary. The bedload-layer model, while slightly more complicated to implement, may provide a more robust solution when working outside of parameter space used to derive the empirical model, since it has a more physical basis. For example, the forward model can explicitly account for gravity and other physical properties of the sediment and fluid. In addition, the bedload-layer model allows for a more mechanistic link between the bedload and suspended load, and avoids uncertainty in how to evaluate the sediment concentration below the reference level. The model might likely be improved by accounting for bedform induced form drag, especially for sand-bedded rivers. That said, more accurate predictions are still achieved with the empirical entrainment relation.

5 Conclusions

We proposed new empirical models for the entrainment of bed material into suspension and for the shape of the concentration profile governed by the Rouse parameter. The models were obtained by regression against suspended sediment data from eight different rivers and six experimental studies. The data cover a wide range of bed material grain sizes (44- 517 µm) and flow depths (0.06-32 m) and include grain-size

specific data with up to 60 size classes. Our analysis of this data suggests that near-bed sediment concentration increases with the ratio between shear velocity and settling velocity (u_{*skin}/w_s or u_*/w_{si}) and Froude number—both parameters also emerge as the key controlling variables in a forward model based on bedload layer concentrations. A parameter such as u_*/w_{si}, which represents the ratio of fluid force to particle settling, was also present in previous relations. The Froude number dependence is less clear; it could be due to stronger sediment-induced stratification in large low-Fr rivers, but our forward model indicates that it emerges because flow velocity and flow depth impact bedload layer concentrations. Our preferred Rouse parameter model for the shape of the concentration profile suggests that sediment concentration is better mixed in the water column with larger u_{*skin}/w_{si} and larger bed friction coefficient, C_f. The Rouse number is not inversely proportional to u_*/w_{si}, unlike standard Rousean theory, indicating that sediment is more stratified than expected with $u_*/w_{si} > \sim 7$ and better mixed than expected with $u_*/w_{si} < \sim 7$, possibly due to the competing effects of sediment-induced stratification when absolute concentrations are large (corresponding to large u_*/w_{si}) and enhanced turbulent mixing when concentration gradients are steep (corresponding to small u_*/w_{si}). The dependence of Rouse number on bed friction coefficient might result from increased turbulence close to the bed in rivers with large bed roughness or bedforms. We also demonstrated that near-bed concentrations can be accurately predicted with saltation equations that have been tested previously for gravel, suggesting a unified framework to model sand and gravel transport in rivers.

Competing interests

The authors declare that they have no conflict of interest.

Data availability

All data used in the analysis are provided in Table S1 of the Supplementary Materials. Model results for all possible variable combinations are given in Table S2.

Author Contributions

MPL and GP conceived the study. JdL compiled data and led data analysis with input from MPL. MPL and JdL wrote the initial manuscript. AJM, DH, JGV and JAN supplied suspended sediment data and contributed to the final manuscript.

Acknowledgements

We thank everyone who has been involved in the suspended sediment data collection in the Yellow River (Brandee Carlson, Hongbo Ma) and the Fraser River (Nicola Rammell, Kate Donkers, Jacqui Brown, Michael Wong, Michelle Linde, and Alex Gitto). This research was sponsored by the National Science Foundation (EAR 1427262) to MPL, JAN and GP. AJM was supported by a NSF Graduate Research Fellowship under EAR 1842494.

Supplementary materials

Table S1 – Contains all the suspended sediment data that was used to find the empirical relations.

Table S2 – All entrainment and Rouse number models ranked according to goodness of fit as indicated by r^2.

References

Akiyama, J.: Entrainment of non cohesive sediment into suspension, in Proc. 3rd Int. Symp. on River Sedimentation, pp. 804–813., 1986.

Ashley, T. C., McElroy, B., Buscombe, D., Grams, P. E., & Kaplinski, M.: Estimating bedload from suspended load and water discharge in sand bed rivers. *Water Resources Research*, 56, e2019WR025883. https://doi.org/10.1029/2019WR025883, 2020.

Allison, M. A. and Meselhe, E. A.: The use of large water and sediment diversions in the lower Mississippi River (Louisiana) for coastal restoration, Journal of Hydrology, 387(3–4), 346–360, doi:10.1016/j.jhydrol.2010.04.001, 2010.

Bennett, S. J., Bridge, J. S. and Best, J. L.: Fluid and sediment dynamics of upper stage plane beds, Journal of Geophysical Research, 103, 1239–1274, 1998.

Bouchez, J., Lupker, M., Maurice, L., Perez, M. and Gaillardet, J.: Prediction of depth-integrated fluxes of suspended sediment in the Amazon River : particle aggregation as a complicating factor, Hydrological Processes, 794 (October 2010), 778–794, doi:10.1002/hyp.7868, 2011.

605

Brownlie, W. R.: Prediction of Flow Depth and Sediment Discharge in Open Channels, California Institute of Technology, 1981.

Burr, D. M., Carling, P. A. and Baker, V. R.: Megaflooding on Earth and Mars, Cambridge University

610 Press., 2009.

Cacchione, D. A., Wiberg, P. L., Lynch, J., Irish, J. and Traykovski, P.: Estimates of suspended-sediment flux and bedform activity on the inner portion of the Eel continental shelf, Marine Geology, 154(1–4), 83–97, 1999.

615

Celik, I. and Rodi, W.: A deposition-entrainment model for suspended sediment transport, Universität Karlsruhe, Karlsruhe, Germany., 1984.

Chatanantavet, P., Whipple, K. X., Adams, M. A. and Lamb, M. P.: Experimental study on coarse grain

620 saltation dynamics in bedrock channels, Journal of Geophysical Research: Earth Surface, 118(2), 1161–1176, doi:10.1002/jgrf.20053, 2013.

Chien, N.: The present status of research on sediment transport, Transactions of the American Society of Civil Engineers, 121(1), 833–868, 1954.

625

Coleman, N. L.: Flume studies on the sediment transport coefficient, Water Resources Research, 6(3), 1970.

Droppo, I. G. and Ongley, E. D.: Flocculation of suspended sediment in rivers of southeastern Canada,

630 Water Research, 28(8), 1799–1809, doi:10.1016/0043-1354(94)90253-4, 1994.

Einstein, H. A.: The Bed-Load Function for Sediment Transportation in Open Channel Flows, Technical Report, Soil Conservation Service,U.S Department of Agriculture, U.S.A, (1026), 1–31, 1950.

635

Einstein, H. A.: Effect of heavy sediment concentration near the bed on velocity and sediment distribution, MRD Sediment Series, University of California, 1955.

Engelund, F. and Fredsøe, J.: A Sediment Transport Model for Straight Alluvial Channels, Nordic

640 Hydrology, 7, 293–306, 1976.

Engelund, F. and Hansen, E.: A Monograph on Sediment Transport in Alluvial Atreams, Danish Tech. Press, Copenhagen, Denmark., 1967.

Ferguson, R. I. and Church, M.: A simple universal equation for grain settling velocity, Journal of
Sedimentary Research, 74(6), 933–937, doi:10.1306/051204740933, 2004.

Fernandez Luque, R. and van Beek, R.: Erosion And Transport Of Bed-Load Sediment, Journal of
Hydraulic Research, 14(2), 127–144, doi:10.1080/00221687609499677, 1976.

Garcia, M.: Sedimentation engineering: processes, measurements, modeling, and practice, Americal
Sociecy of Civil Engineers, Manual 110, 2008.

Garcia, M. and Parker, G.: Entrainment of Bed Sediment into Suspension, Journal of Hydraulic
Engineering, 117(4), 414–435, doi:10.1061/(ASCE)0733-9429(1991)117:4(414), 1991.

Gitto, A. B., Venditti, J. G., Kostaschuk, R. and Church, M.: Representative point-integrated suspended
sediment sampling in rivers, Water Resources Research, 53(4), 2956–2971,
doi:10.1002/2016WR019187, 2017.

Graf, W. H. and Cellino, M.: Suspension flows in open channels; experimental study, Journal of
Hydraulic Research, 40(4), 435–447, doi:10.1080/00221680209499886, 2002.

Greimann, B. P. and Holly Jr, F. M.: Two-phase flow analysis of concentration profiles, Journal of
hydraulic Engineering, 127(9), 753–762, 2001.

Hartshorn, K., Hovius, N., Dade, W. B. and Slingerland, R. L.: Climate-driven bedrock incision in an
active mountain belt, Science, 297(5589), 2036–2038, doi:10.1126/science.1075078, 2002.

Haught, D., Venditti, J. G. and Wright, S. A.: Calculation of in situ acoustic sediment attenuation using
off-the-shelf horizontal ADCPs in low concentration settings, Water Resources Research, 53(6), 5017–
5037, doi:10.1002/2016WR019695, 2017.

Lamb, M. P. and Venditti, J. G.: The grain size gap and abrupt gravel-sand transitions in rivers due to
suspension fallout, Geophysical Research Letters, 43(8), 3777–3785, doi:10.1002/2016GL068713,
2016.

Lamb, M. P., Dietrich, W. E. and Sklar, L. S.: A model for fluvial bedrock incision by impacting
suspended and bed load sediment, Journal of Geophysical Research: Earth Surface, 113(3), 1–18,
doi:10.1029/2007JF000915, 2008a.

Lamb, M. P., Dietrich, W. E. and Venditti, J. G.: Is the critical shields stress for incipient sediment
motion dependent on channel-bed slope?, Journal of Geophysical Research: Earth Surface, 113(2), 1–
20, doi:10.1029/2007JF000831, 2008b.

Lamb, M. P., Brun, F. and Fuller, B. M.: Direct measurements of lift and drag on shallowly submerged

cobbles in steep streams: Implications for flow resistance and sediment transport, Water Resources Research, 53(9), 7607–7629, doi:10.1002/2017WR020883, 2017.

Larsen, I. J. and Lamb, M. P.: Progressive incision of the Channeled Scablands by outburst floods, Nature, 538(7624), 229–232, doi:10.1038/nature19817, 2016.

Lupker, M., France-Lanord, C., Lavé, J., Bouchez, J., Galy, V., Métivier, F., Gaillardet, J., Lartiges, B. and Mugnier, J. L.: A Rouse-based method to integrate the chemical composition of river sediments: Application to the Ganga basin, Journal of Geophysical Research: Earth Surface, 116(4), 1–24, doi:10.1029/2010JF001947, 2011.

Ma, H., Nittrouer, J. A., Naito, K., Fu, X., Zhang, Y., Moodie, A. J., Wang, Y., Wu, B. and Parker, G.: The exceptional sediment load of fine-grained dispersal systems : Example of the Yellow River , China, Science Advances, 3, 1–8, 2017.

McLean, S. R.: Depth-integrated suspended-load calculations, Journal of Hydraulic Engineering, 117(11), 1440–1458, 1992.

Mellor, G. L. and Yamada, T.: Development of a turbulence closure model for geophysical fluid problems, Reviews of Geophysics, 20(4), 851–875, 1982.

Moodie, A. J.: Yellow River Kenli Lijin Station Survey, doi:10.5281/zenodo.3457639, 2019.

Muste, M., Yu, K., Fujita, I. and Ettema, R.: Two-phase versus mixed-flow perspective on suspended sediment transport in turbulent channel flows, Water Resources Research, 41(10), doi:10.1029/2004WR003595, 2005.

Mutsert, K. De, Lewis, K., Milroy, S., Buszowski, J. and Steenbeek, J.: Using ecosystem modeling to evaluate trade-offs in coastal management : Effects of large-scale river diversions on fish and fisheries, Ecological Modelling, 360, 14–26, doi:10.1016/j.ecolmodel.2017.06.029, 2017.

Nielsen, P. and Teakle, I. A. .: Turbulent diffusion of momentum and suspended particles : A finite-mixing-length theory, Physics of Fluids, 16(7), 2342–2348, doi:10.1063/1.1738413, 2004.

Nittrouer, C. A., Curtin, T. B. and DeMaster, D. J.: Concentration and flux of suspended sediment on the Amazon continental shelf, Continental Shelf Research, 6(1–2), 151–174, 1986.

Paola, C. and Voller, V. R.: A generalized Exner equation for sediment mass balance, Journal of Geophysical Research, 110, 1–8, doi:10.1029/2004JF000274, 2005.

Paola, C., Parker, G., Seal, R., Sinha, S. K., Southard, J. B. and Wilcock, P. R.: Downstream fining by selective deposition in a laboratory flume, Science, 258(5089), 1757–1760,

doi:10.1126/science.258.5089.1757, 1992.

730 Parker, G.: Self-formed straight rivers with equilibrium banks and mobile bed . Part 1. The sand-silt river, Journal of Fluid Mechanics, 89, 109–125, 1978.

Parker, G.: Surface-based bedload transport relation for gravel rivers, Journal of Hydraulic Research, 28(4), 417–436, doi:10.1080/00221689009499058, 1990.

735

Parker, G., Klingeman, P. C. and McLean, D. G.: Bedload and size distribution in paved gravel-bed streams., Journal of the Hydraulics Division-Asce, 108(HY4), 544–571, 1982.

van Rijn, L.: Sediment transport, part 2: Suspended load transport, Journal of Hydraulic Engineering, 740 110(11), 1613–1641, 1984.

Rouse, H.: Modern Conceptions of the Mechanics of Fluid Turbulence, Transactions of the American Society of Civil Engineers, 102(1), 463–505, 1937.

745 Santini, W., Camenen, B., Coz, J. Le, Vauchel, P., Guyot, J. and Santini, C. W.: An index concentration method for suspended load monitoring in large rivers of the Amazonian foreland, Earth Surface Dynamics, 7, 515–536, 2019.

Scheingross, J. S., Brun, F., Lo, D. Y., Omerdin, K. and Lamb, M. P.: Experimental evidence for fluvial 750 bedrock incision by suspended and bedload sediment, Geology, 42(6), 523–526, doi:10.1130/G35432.1, 2014.

Sklar, L. S. and Dietrich, W. E.: A mechanistic model for river incision into bedrock by saltating bed load, Water Resources Research, 40(6), 1–22, doi:10.1029/2003WR002496, 2004.

755

Smith, J. D. and Mclean, S. R.: Spatially Averaged Flow Over a Wavy Surface, Journal of Geophysical Research, 82(12), 1735–1746, 1977.

Syvitski, J. P. M., Vo, C. J., Kettner, A. J. and Green, P.: Impact of humans on the flux of terrestrial 760 sediment to the global coastal ocean, Science, 308, 376–381, 2005.

Vanoni, V. a.: Transportation of Suspended Sediment by Water, Transactions of the American Society of Civil Engineers, 111(1), 67–102, 1946.

765 Vanoni, V. A.: Factors determining bed forms of alluvial streams, Journal of the Hydraulics Division, 100(hy3), 1974.

Walling, D. E.: Human impact on land – ocean sediment transfer by the world's rivers, Geomorphology, 79, 192–216, doi:10.1016/j.geomorph.2006.06.019, 2006.

770   Wilcock, P. R. and Crowe, J. C.: Surface-based Transport Model for Mixed-Size Sediment, Journal of Hydraulic Engineering, 129(2), 120–128, doi:10.1061/(ASCE)0733-9429(2003)129, 2003.

Winterwerp, J. C.: Stratification effects by fine suspended sediment at low, medium, and very high concentrations, Journal of Geophysical Research: Oceans, 111(5), 1–11, doi:10.1029/2005JC003019, 775   2006.

Wright, S. and Parker, G.: Density Stratification Effects in Sand-Bed Rivers, Journal of Hydraulic Engineering, 130(August), 783–795, doi:10.1061/(ASCE)0733-9429(2004)130:8(783), 2004a.

780   Wright, S. and Parker, G.: Flow Resistance and Suspended Load in Sand-Bed Rivers: Simplified Stratification Model, Journal of Hydraulic Engineering, 130(8), 796–805, doi:10.1061/(ASCE)0733-9429(2004)130:8(796), 2004b.

York, D.: Least squares fitting of a straight line with correlated errors, Earth and planetary science 785   letters, 5, 320–324, 1968.

790

Table 1. Previous relations for the factor β.

Source	Formula	Parameters
van Rijn, 1984	$\beta = 1 + 2\left(\dfrac{w_s}{u_*}\right)^2 \quad for \ 0.1 < \dfrac{w_s}{u_*} < 1$	u_*/w_s
Graf & Cellino, 2002	$\beta = \dfrac{3}{10} + \dfrac{3}{4}\dfrac{w_s}{u_*} \quad for \ 0.2 < \dfrac{w_s}{u_*} < 0.6 \ and \ no \ bedforms$ $\beta = 1 + 2\left(\dfrac{w_s}{u_*}\right)^2 \quad for \ 0.1 < \dfrac{w_s}{u_*} < 1 \ and \ bedforms$	u_*/w_s
Wright & Parker, 2004	$\beta = \begin{cases} 1 - 0.06\left(\dfrac{C_a}{S}\right)^{0.77} & for \ \dfrac{C_a}{S} \leq 10 \\ 0.67 - 0.0025\left(\dfrac{C_a}{S}\right) & for \ \dfrac{C_a}{S} > 10 \end{cases}$	C_a/S
Santini et al., 2019 (modified from Rose & Thorne, 2001)	$\beta = 3.1 \, exp\left[-0.19 \times 10^{-3} \dfrac{u_*}{w_s}\left(\dfrac{H}{D}\right)^{0.6}\right] + 0.16$	$u_*/w_s, \ H/D$

Table 2. Previous relations for sediment entrainment, E_s.

Source	Formula	Parameters	Reference height	Grain-size distribution
Einstein, 1950	$$E_s = \frac{1}{23.2}\frac{q_*}{(\tau_{*skin})^{0.5}}$$ $$q_* = 3.97(\tau_{*skin} - 0.0495)^{1.5}$$	τ_{*skin}	$2D$	Uniform
Engelund & Fredsøe, 1976	$$E_s = \frac{0.65}{(1 + \lambda_b^{-1})^3}$$ $$\lambda_b = \left[\frac{\tau_{*skin} - 0.06 - \frac{\beta p \pi}{6}}{0.027(R+1)\tau_{*skin}}\right]^{0.5}$$ $$p = \left[1 + \left(\frac{\frac{\pi}{6}}{\tau_{*skin} - 0.06}\right)^4\right]^{-0.25}$$ $$\beta = 1$$	τ_{*skin}	$2D$	Uniform
Smith & McLean, 1977	$$E_s = \frac{0.65\gamma_0 S_0}{1 + \gamma_0 S_0}$$ $$S_0 = \frac{\tau_{*skin} - \tau_{*c}}{\tau_{*c}}$$ $$\gamma_0 = 2.4 \cdot 10^{-3}$$ τ_{*c} is calculated with Brownlie (1981): $$\tau_{*c} = 0.22 Re_p^{-0.6} + 0.06 \cdot 10^{(-7.7 Re_p^{-0.6})}$$	τ_{*skin}, τ_{*c}	$\alpha_0(\tau_{skin}^* - \tau_c^*)D + k_s$ $\alpha_0 = 26.3$	Uniform
van Rijn, 1984	$$E_s = 0.015\frac{D}{a}\frac{S_0^{1.5}}{D_*^{0.3}}$$ $$\text{with: } S_0 = \frac{\tau_{*skin} - \tau_{*c}}{\tau_{*c}}$$ $$\text{and: } D_* = D\left(\frac{gR}{v}\right)^{1/3}$$	$\tau_{*skin}, \tau_{*c}, D$	One half bedform height or k_s, with a minimum of $0.01H$	Uniform
Celik & Rodi, 1984	$$E_s = \frac{k_0\bar{C}}{I}$$ $$\bar{C} = 0.034\left[1 - \left(\frac{k_s}{H}\right)^{0.06}\right]\frac{u_*^2}{gRH}\frac{U}{w_s}$$ $$I = \int_{0.05}^{1}\left(\frac{1-\eta}{\eta}\cdot\frac{\eta_b}{1-\eta_b}\right)^{w_s/0.4u_*}d\eta$$ $$k_0 = 1.13, \eta = \frac{z}{H}, \eta_b = 0.05$$	D, k_s, u_*, U, w_s, H	$0.05H$	Uniform

Akiyama & Fukushima, 1986	$E_s = 0; Z < Z_c$ $E_s = 3 \times 10^{-12} Z^{10}\left(1 - \dfrac{Z_c}{Z}\right); Z_c < Z < Z_m$ $Z = \dfrac{u_*}{w_s} Re_p^{0.5}$ $Z_c = 5; Z_m = 13.2$	$u_*,\ w_s,\ Re_p$	$0.05H$	Uniform
Garcia & Parker, 1991	$E_{si} = \dfrac{A(\lambda X_i)^5}{1 + \dfrac{A}{0.3}(\lambda X_i)^5}$ $X_i = \left(\dfrac{u_{*skin}}{w_{si}} Re_{pi}^{0.6}\right)\left(\dfrac{D_i}{D_{50}}\right)^{0.2}$ $A = 1.3 \cdot 10^{-7}$ $\lambda = 1 - 0.288\sigma_\phi$ σ_ϕ is the geometric standard deviation of bed material sizes	$u_{*skin},\ w_{si},\ Re_{pi},$ $D_i/D_{50},\ \sigma_\phi$	$0.05H$	Mixtures
McLean, 1992	$E_{si} = E_s p_{sbi}$ $E_s = \dfrac{0.65\gamma_0 S_0}{1 + \gamma_0 S_0},$ $S_0 = \dfrac{\tau_{*skin} - \tau_{*c}}{\tau_{*c}}$ $\gamma_0 = 0.004$ $p_{sbi} = \dfrac{\varphi_i f_i}{\sum_{n=1}^{N} \varphi_i f_i}$ $\varphi_i = 1\ for: u_* > w_{si}$ $\varphi_i = \dfrac{u_* - u_{*cr}}{w_{si} - u_{*cr}}\ for: u_* < w_{si}$	$\tau_{*c},\ \tau_{*skin},\ u_*,$ $w_{si},\ f_i$	See original publication	Mixtures
Wright & Parker, 2004	$E_{si} = \dfrac{B(\lambda X_i)^5}{1 + \dfrac{B}{0.3}(\lambda X_i)^5}$ $with:\ X_i = \left(\dfrac{u_{*skin}}{w_{si}} Re_{pi}^{0.6}\right) S^{0.08}\left(\dfrac{D_i}{D_{50}}\right)^{0.2}$ $B = 7.8 \cdot 10^{-7}$ $\lambda = 1 - 0.28\sigma_\phi$ σ_ϕ is the geometric standard deviation of bed material sizes	$u_{*skin},\ w_{si},\ Re_{pi},$ $S,\ D_i/D_{50},\ \sigma_\phi$	$0.05H$	Mixtures

Table 3: Summary of experimental and field datasets included in the database.

Data source	Type	Location	Median bed material grain size, D_{50} (µm)	Water depth, H (m)	Number of grain size classes	Number of profiles
Jordan [1965]	river	Mississippi at St Louis	189-457	3.54-16.34	12	51
Nitrouer et al. [2011]	river	Mississippi at Empire reach	166-244	12.96-32.38	43	9
Lupker et al. [2011]	river	Ganges at Harding bridge	159-268	10.0-14.0	31	7
Nordin & Dempster [1963]	river	Rio Grande	166-439	0.2-0.78	12	23
Moodie [2019]	river	Yellow River	44-112	1.55-7.65	51	35
Haught et al. [2017]	river	Fraser River	300	8.7-14.5	60	25
Hubbell & Matejka [1959]	river	Middle Loup River	313-517	0.33-1.19	10	20
Colby & Hembree [1955]	river	Niobrara River	226-305	0.24-0.7	7	10
Brooks [1954]	experiments	-	160	0.059-0.085	1	7
Barton & Lin [1955]	experiments	-	180	0.091-0.42	1	29
Coleman [1981]	experiments	-	105-400	0.17	1	3
Lyn [1986]	experiments	-	150-240	0.065	1	3
Sumer [1996]	experiments	-	130	0.1	1	3
Cellino [1998]	experiments	-	135-210	0.12	1	17

Table 4: One-, two- and three-parameter models for Rouse number of the form $P_i = AP_1^{e_1} P_2^{e_2} P_3^{e_3}$. The two best-fitting versions of each model are shown, one with u_* and one with u_{*skin}, and the shaded row is the best fitting of the two (highest r^2). See Table S2 for all model fits.

Number of model parameters	r^2	P_1	P_2	P_3	A	e_1	e_2	e_3
1	0.325	u_*/w_{si}	-	-	0.991	-0.453	-	-
	0.225	u_{*skin}/w_{si}	-	-	0.718	-0.372	-	-
2	0.396	u_{*skin}/w_{si}	C_f	-	0.145	-0.459	-0.300	-
	0.378	u_*/w_{si}	C_f	-	0.387	-0.438	-0.161	-
3	0.426	u_{*skin}/w_{si}	C_f	C_a/S	0.285	-0.514	-0.212	0.0811
	0.39	u_*/w_{si}	C_f	H/D	0.274	-0.459	-0.141	0.0485

Table 5: One-, two- and three-parameter models for the entrainment parameter of the form $E_{si} = AP_1^{e_1} P_2^{e_2} P_3^{e_3}$. The two best-fitting versions of each model are shown, one with $\boldsymbol{u_*}$ and one with $\boldsymbol{u_{*skin}}$, and the shaded row is the best fitting of the two (highest r^2). See Table S2 for all model fits.

Number of model parameters	r^2	P_1	P_2	P_3	A	e_1	e_2	e_3
1	0.61	u_{*skin}/w_{si}	-	-	4.23E-05	1.94	-	-
	0.33	u_*/w_{si}	-	-	3.66E-05	1.44	-	-
2	0.79	u_{*skin}/w_{si}	Fr	-	4.74E-04	1.77	1.18	-
	0.74	u_*/w_{si}	Fr	-	7.04E-04	1.71	1.81	-
3	0.80	u_*/w_{si}	Fr	R_{pi}	5.73E-03	1.31	1.59	-0.86
	0.79	u_{*skin}/w_{si}	Fr	S	2.93E-04	1.75	1.31	-0.079

Table 6: Coefficient of determination (r^2) of grain-size specific sediment concentration at each sample elevation in the water column for different combinations of models for the entrainment, E_{si}, and Rouse, P_i, parameters. The favored model combination is highlighted in grey.

Goodness of fit (r^2)		Entrainment parameter model, E_{si}					
		Best fit 1-parameter model containing u_*/w_{si}	Best fit 1-parameter model containing u_{*skin}/w_{si}	Best fit 2-parameter model containing u_*/w_{si}	Best fit 2-parameter model containing u_{*skin}/w_{si}	Best fit 3-parameter model containing u_*/w_{si}	Best fit 3-parameter model containing u_{*skin}/w_{si}
Rouse parameter model, P_i	Best fit 1-parameter model containing u_*/w_{si}	0.646	0.768	0.862	0.873	0.878	0.871
	Best fit 1-parameter model containing u_{*skin}/w_{si}	0.676	0.786	0.859	0.867	0.872	0.865
	Best fit 2-parameter model containing u_*/w_{si}	0.634	0.768	0.856	0.876	0.878	0.876
	Best fit 2-parameter model containing u_{*skin}/w_{si}	0.659	0.785	0.853	0.875	0.875	0.875
	Best fit 3-parameter model containing u_*/w_{si}	0.637	0.757	0.802	0.818	0.819	0.817
	Best fit 3-parameter model containing u_{*skin}/w_{si}	0.637	0.766	0.849	0.868	0.870	0.868
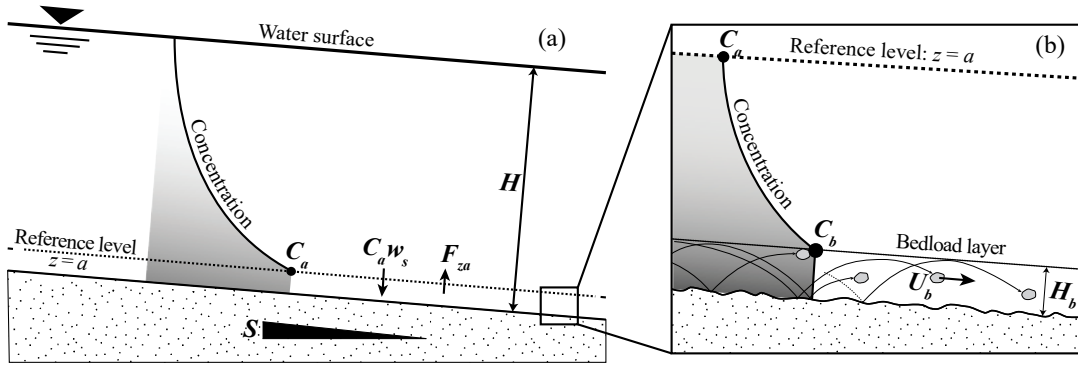
Figure 1: a) Conceptual diagram of suspended sediment concentration-depth profile of a river of depth H and bed slope S, showing the volumetric sediment concentration, C_a, settling flux per unit bed area, $C_a w_s$, and entrainment flux per unit bed area, F_{za}, at the reference level of $z = a$, in which $z = 0$ is bed elevation. b) Near-bed zone below the reference level showing the bedload layer with concentration C_b, bedload velocity U_b and bedload-layer height H_b.
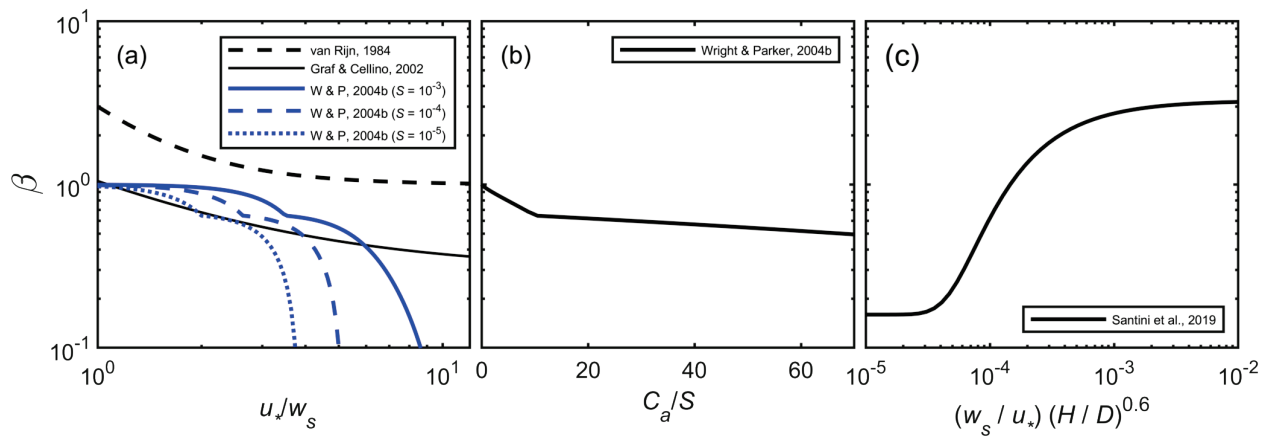
Figure 2: Existing relations for the factor β (Eq. 2) as a function of a) shear velocity normalized by setting velocity u_*/w_s (van Rijn, 1985; Graf and Celino, 2002; Wright and Parker, 2004b), b) near-bed concentration normalized by slope C_a/S (Wright and Parker, 2004b), and c) w_s/u_* $(H / D)^{0.6}$ as proposed by Santini et al. (2019). In panel (a), the Wright and Parker relation (denoted W & P) used C_a calculated from the entrainment relation of Wright & Parker (2004b).
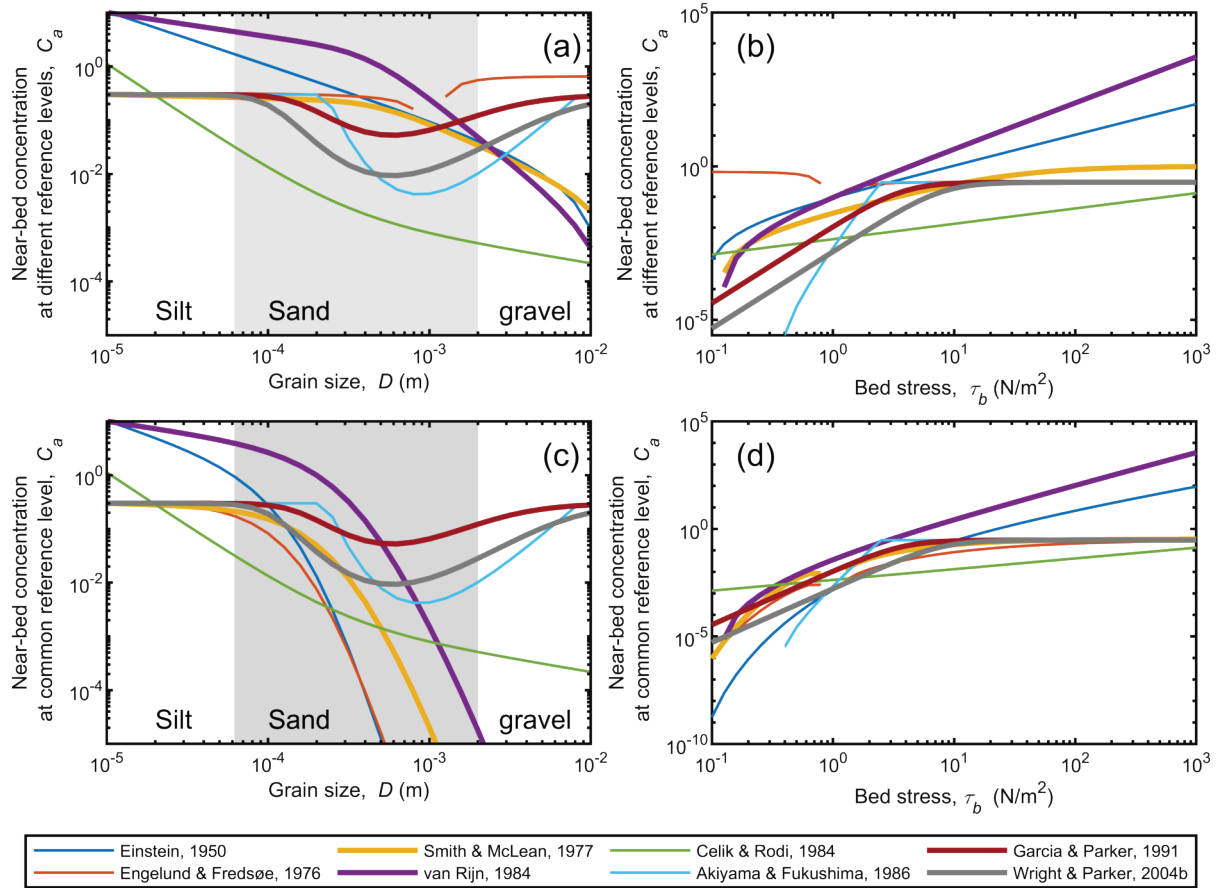
Figure 3: Existing relations for near-bed suspended sediment concentration under equilibrium conditions (i.e., $E_s = C_a$) at the reference level, $z = a$, specified by each study as a function of a) grain size and b) bed stress. In panels (c) and (d) the predicted concentrations are interpolated to a common reference level, $a = 0.05H$, using the Rouse equation with $\beta = 1$ to better compare models.
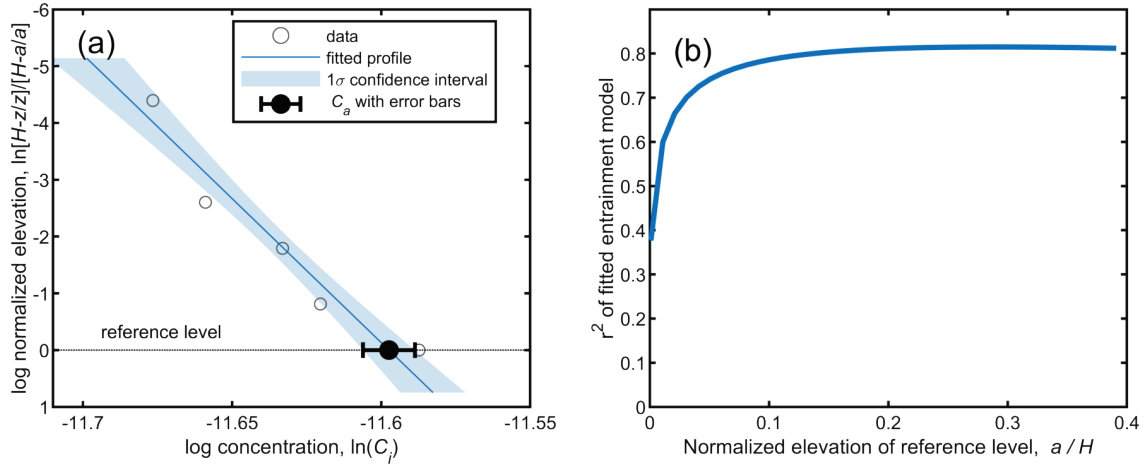
Figure 4: a) Example of suspended sediment data linearized in Rouse coordinates with a fitted Rouse profile (Eq. 1), in which z is the elevation above the bed, H is the flow depth, extrapolation to the reference level at $z = a$ gives the reference concentration, C_a. b) Effect of choice of reference level elevation on r^2 of the best fit entrainment relation, E_{si}, to the data.
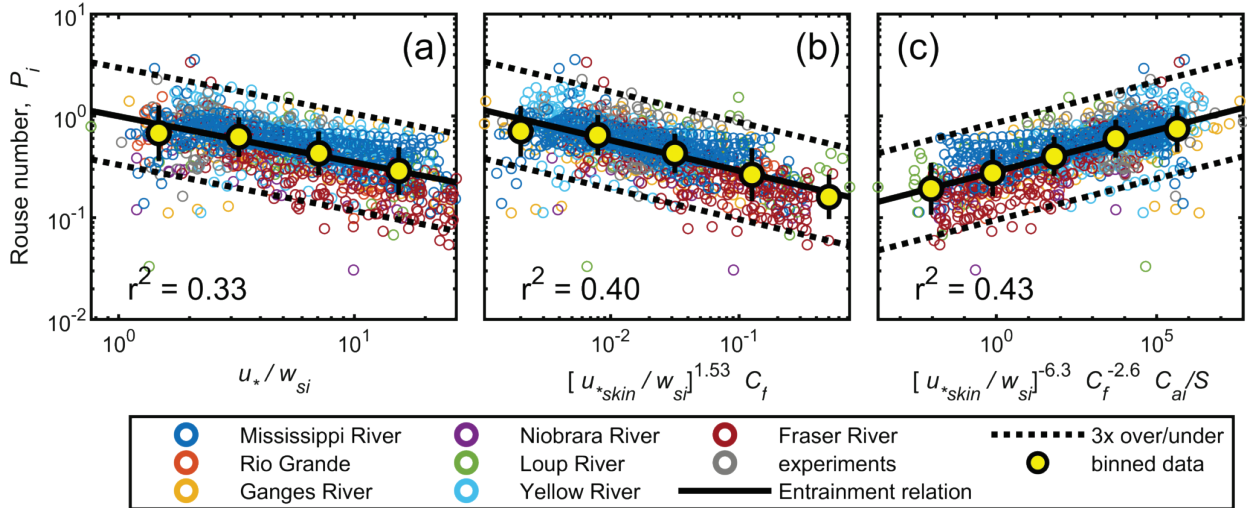
Figure 5: Best-fit models for Rouse number for grain-size specific data with one parameter (a), two parameters (b) and three parameters (c); equations are highlighted grey in Table 4. The plotting is done such that the exponent on the last parameter is unity (e.g., Eq. (23) on panel b is rewritten

as $P_i = \left(0.145^{1/-0.3} \left(\dfrac{u_{*skin}}{w_{si}} \right)^{-0.46/-0.3} C_f \right)^{-0.3}$) to allow comparison to plots of Garcia & Parker

(1991) and Wright & Parker (2004b). Yellow filled symbols are the geometric mean and the error bars indicate the geometric standard deviation within each arbitrary spaced bin.
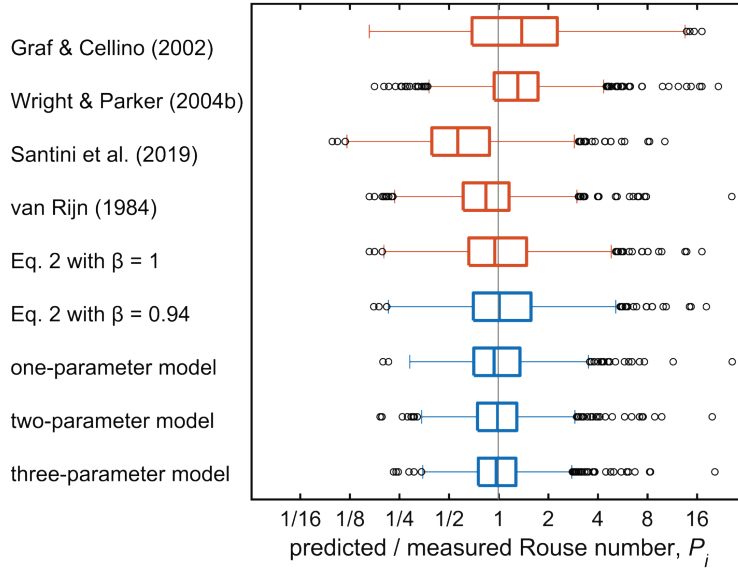
Figure 6: Boxplot of predicted versus measured Rouse number, P_i, for our models and previous models. The best-fit one, two and three parameter models correspond to the equations in Table 4 that are highlighted in grey.
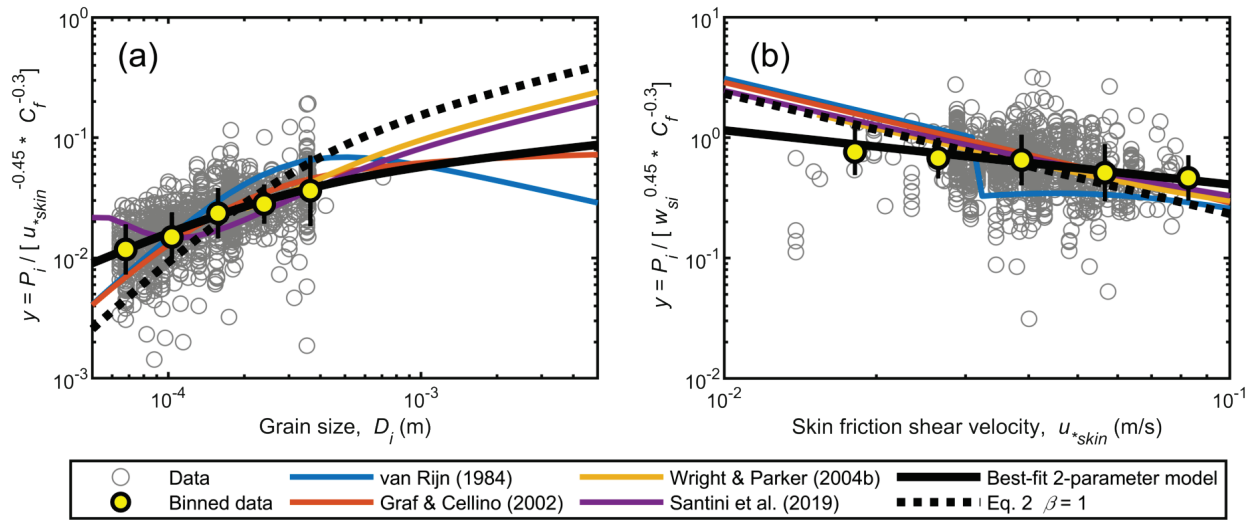
Figure 7: Rouse number, P_i, has been normalized to isolate the effect of a) grain size and b) skin-friction shear velocity to check for spurious correlation. Yellow filled symbols are the geometric mean and the error bars indicate the geometric standard deviation within each bin. The best-fit two parameter model is Eq. (22).
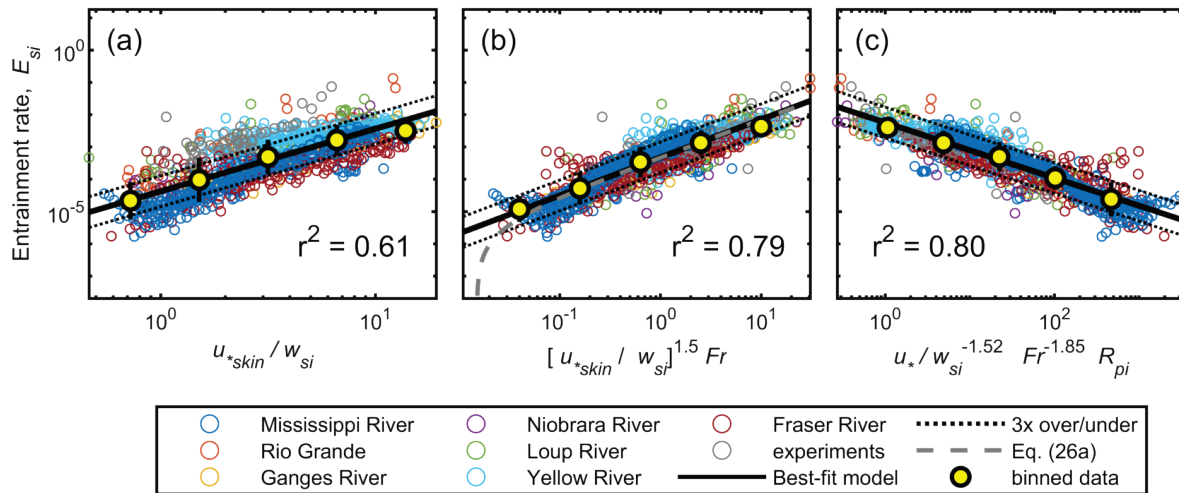
Figure 8: Best-fit models for the dimensionless entrainment rate, E_{si}, for grain-size specific data with one parameter (a), two parameters (b) and three parameters (c); equations are highlighted grey in Table 5. The plotting is done such that the exponent on the last parameter is unity to allow comparison to plots of Garcia & Parker (1991) and Wright & Parker (2004b). Yellow filled symbols are the geometric mean and the error bars indicate the geometric standard deviation within each bin.
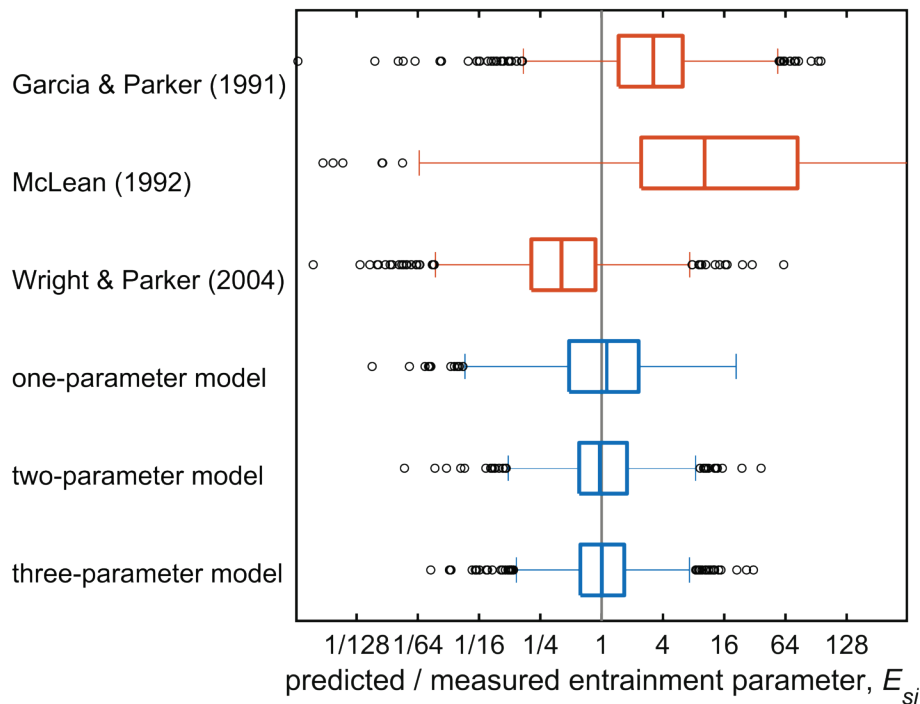
Figure 9: Boxplot of predicted versus measured entrainment parameters, E_{si}, for our models and previous models. The best-fit one, two and three parameter models correspond to the equations in Table 5 that are highlighted in grey.
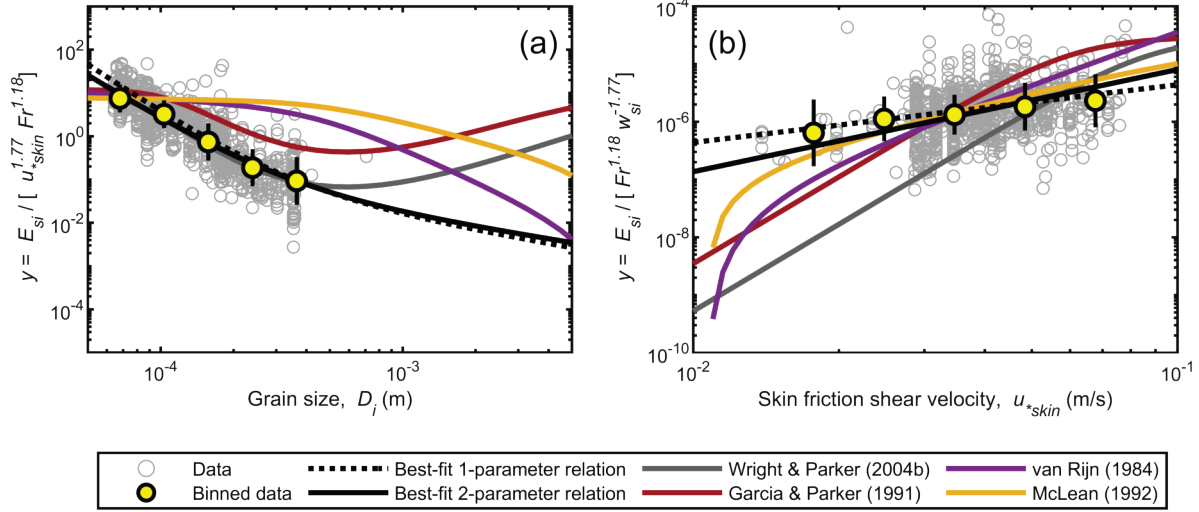
Figure 10: Entrainment parameter, E_{si}, normalized to isolate the effect of a) grain size and b) skin-friction shear velocity to check for spurious correlation. Yellow filled symbols are the geometric mean and the error bars indicate the geometric standard deviation within each bin. The best-fit models are Eqs. (24) and (25).
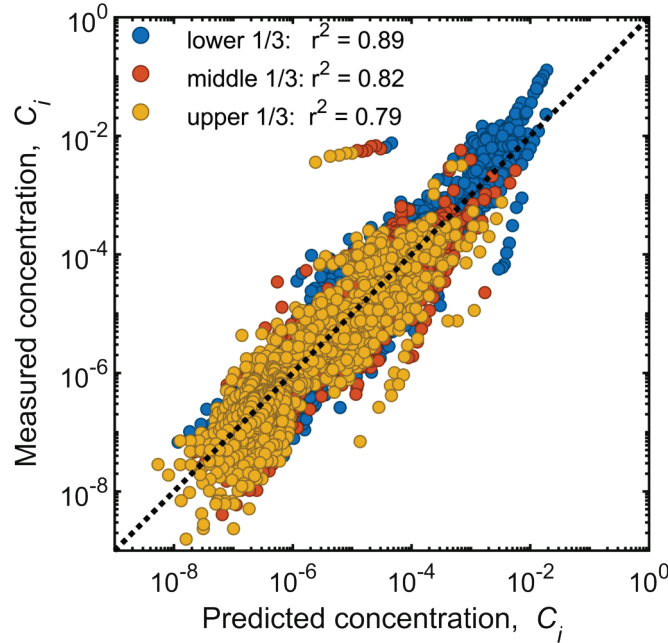
Figure 11: Measured versus predicted grain-size specific concentration for each sample in the water column. Colors indicate the relative elevation in the water column of each sample. The predictions are from the two-parameter model to predict the entrainment rate ($E_{si} = 4.74 \times 10^{-4} \left(\frac{u_{*skin}}{w_{si}}\right)^{1.77} Fr^{1.18}$) and the one-parameter model for the Rouse number ($P_i = (u_*/w_{si})^{-0.45}$).
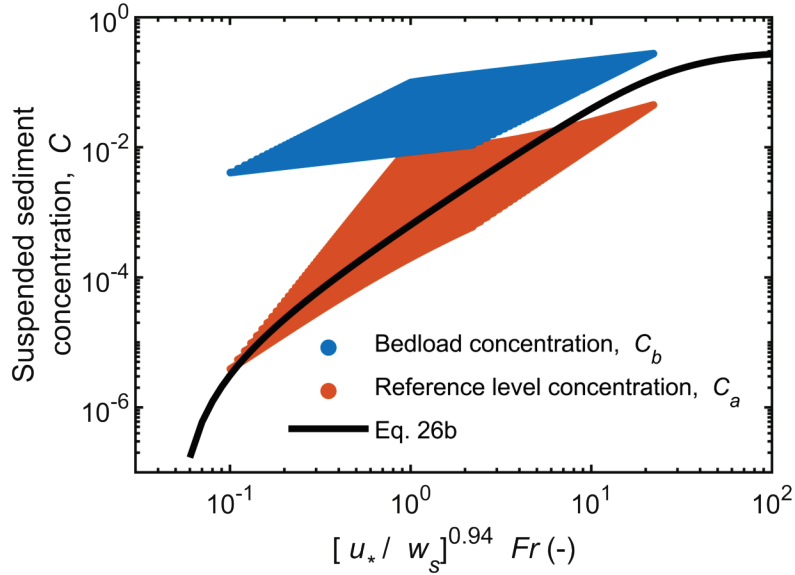
Figure 12. Best fit two parameter model for sediment entrainment without form drag, Eq. (26b), presented here for uniform gravel. The plotting is done such that the exponent on the last parameter is unity to allow comparison to plots of Garcia & Parker (1991) and Wright & Parker (2004b). The colored regions are prediction envelopes for synthetic gravel data using the bedload-layer equations to estimate the bedload volumetric concentration, C_b, and the Rouse profile to interpolate higher in the water column to the reference level at $z = 0.1H$ (C_a). The synthetic data envelope represents a wide range of parameter space: $0.1 < Fr < 1$ and $1 < \tau_* < 1000$.
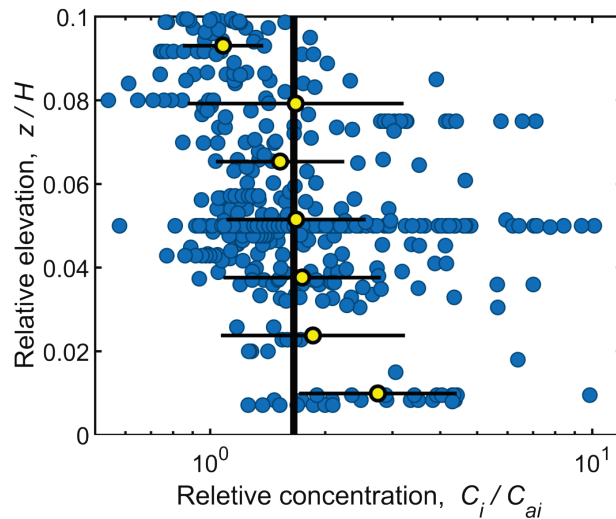
Figure 13: Grain-size specific concentration, C_i, from the lowest 10% of the flow (i.e., below the reference level $z = 0.1H$) relative to the concentration at the reference level, C_{ai}, as a function of depth above the bed, z, relative to the flow depth, H. Yellow filled symbols are the geometric mean and the error bars indicate the geometric standard deviation within each elevation bin, and the black line is the geometric mean of all data representing $C_i = 1.66 C_{ai}$.
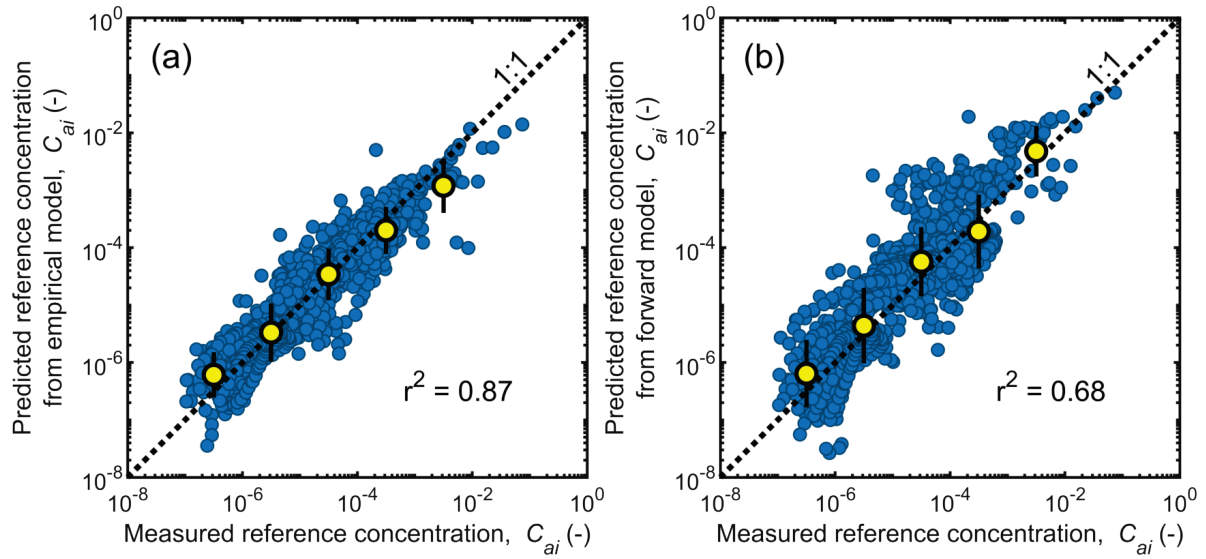
Figure 14: Measured versus predicted grain-size specific near-bed concentration, C_{ai}, at the reference level $z = 0.1H$ for a) our two-parameter empirical relation (Eq. 25) and b) for the forward modelling approach using the bedload-layer equations (Section 4.3). Data (blue markers) are from the entire data base of suspended sand described in Section 2.1 (Table S1) are at $z = 0.1H$. Yellow symbols are the geometric mean and the error bars indicate the geometric standard deviation within each bin.